

2007

# Corrosion protection using conducting polymers

Jan Magnus Gustavsson  
*University of Wollongong*

**UNIVERSITY OF WOLLONGONG**

**COPYRIGHT WARNING**

You may print or download ONE copy of this document for the purpose of your own research or study. The University does not authorise you to copy, communicate or otherwise make available electronically to any other person any copyright material contained on this site. You are reminded of the following:

This work is copyright. Apart from any use permitted under the Copyright Act 1968, no part of this work may be reproduced by any process, nor may any other exclusive right be exercised, without the permission of the author.

Copyright owners are entitled to take legal action against persons who infringe their copyright. A reproduction of material that is protected by copyright may be a copyright infringement. A court may impose penalties and award damages in relation to offences and infringements relating to copyright material. Higher penalties may apply, and higher damages may be awarded, for offences and infringements involving the conversion of material into digital or electronic form.

**Unless otherwise indicated, the views expressed in this thesis are those of the author and do not necessarily represent the views of the University of Wollongong.**

## Recommended Citation

Gustavsson, Jan Magnus, Corrosion protection using conducting polymers, PhD thesis, Department of Chemistry, University of Wollongong, 2007. <http://ro.uow.edu.au/theses/656>

Research Online is the open access institutional repository for the University of Wollongong. For further information contact the UOW Library: [research-pubs@uow.edu.au](mailto:research-pubs@uow.edu.au)

## **NOTE**

This online version of the thesis may have different page formatting and pagination from the paper copy held in the University of Wollongong Library.

## **UNIVERSITY OF WOLLONGONG**

### **COPYRIGHT WARNING**

You may print or download ONE copy of this document for the purpose of your own research or study. The University does not authorise you to copy, communicate or otherwise make available electronically to any other person any copyright material contained on this site. You are reminded of the following:

Copyright owners are entitled to take legal action against persons who infringe their copyright. A reproduction of material that is protected by copyright may be a copyright infringement. A court may impose penalties and award damages in relation to offences and infringements relating to copyright material. Higher penalties may apply, and higher damages may be awarded, for offences and infringements involving the conversion of material into digital or electronic form.

**CORROSION PROTECTION USING  
CONDUCTING POLYMERS**

A thesis submitted in fulfilment of the requirements  
for the award of the degree

**DOCTOR OF PHILOSOPHY**

from the

**UNIVERSITY OF WOLLONGONG**

by

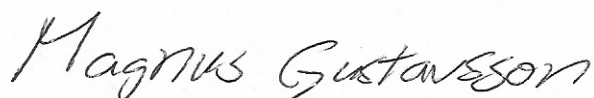
**JAN MAGNUS GUSTAVSSON, B.Sc., M.Sc.**

**ACES  
DEPARTMENT OF CHEMISTRY**

March 2006

## CERTIFICATION

I, Magnus Gustavsson, declare that this thesis, submitted in fulfilment of the requirements for the award of Doctor of Philosophy, in the Department of Chemistry, University of Wollongong, is wholly my own work unless otherwise referenced or acknowledged. The document has not been submitted for qualifications at any other university or institution.

A handwritten signature in black ink that reads "Magnus Gustavsson". The signature is written in a cursive style with a capital 'M' and 'G'.

Magnus Gustavsson

31 March 2006.

# TABLE OF CONTENTS

<b>CERTIFICATION</b>	<b>I</b>
<b>TABLE OF CONTENTS</b>	<b>II</b>
<b>LIST OF FIGURES</b>	<b>X</b>
<b>LIST OF TABLES</b>	<b>XXV</b>
<b>ABSTRACT</b>	<b>XXVII</b>
<b>ACKNOWLEDGMENTS</b>	<b>XXIX</b>
<b>CHAPTER 1- GENERAL INTRODUCTION</b>	<b>1</b>
<b>1.1 BACKGROUND</b>	<b>1</b>
<b>1.2 INTRODUCTION TO CORROSION</b>	<b>2</b>
<i>1.2.1 Cathodic protection</i>	<i>4</i>
<i>1.2.2 Anodic protection</i>	<i>4</i>
<i>1.2.3 Chemical inhibition</i>	<i>5</i>
<b>1.3 CORROSION OF ALUMINIUM ALLOY AA2024-T3</b>	<b>5</b>
<i>1.3.1 Corrosion protection of Aluminium Alloy AA2024-T3</i>	<i>7</i>
<b>1.4 CORROSION OF ZINC-55% ALUMINIUM HOT DIP COATED STEEL</b>	<b>9</b>
<i>1.4.1 Corrosion of zinc</i>	<i>9</i>

<i>1.4.2 Corrosion protection of galvanic coatings</i>	10
<b>1.5 INTRINSICALLY CONDUCTING POLYMERS (ICP)</b>	<b>10</b>
<b>1.6 SYNTHESIS</b>	<b>13</b>
<i>1.6.1 Polypyrrole</i>	14
<i>1.6.2 Polyaniline</i>	15
<i>1.6.3 General properties of Polypyrrole</i>	17
<i>1.6.4 General properties of Polyaniline</i>	19
<i>1.6.5 Processing of ICP</i>	20
<i>1.6.6 ICP for corrosion control of aluminium alloys</i>	21
<b>1.7 RESEARCH AIM</b>	<b>25</b>
<b>CHAPTER 2- REVIEW OF RELEVANT TECHNIQUES</b>	<b>27</b>
<b>2.1 INTRODUCTION</b>	<b>27</b>
<b>2.2 DC TECHNIQUES</b>	<b>28</b>
<i>2.2.1 Open Circuit Potential</i>	28
<i>2.2.2 Potentiodynamic polarisation</i>	29
<b>2.3 ELECTROCHEMICAL IMPEDANCE SPECTROSCOPY (EIS)</b>	<b>31</b>
<i>2.3.1 EIS experiment</i>	33
<i>2.3.2 EIS analysis</i>	34
<i>2.3.3 Equivalent circuit</i>	37
<i>2.3.4 EC Fitting</i>	38
<i>2.3.5 EC of a corroding metal</i>	39
<i>2.3.6 EIS of a polymer coated metal</i>	41
<b>2.4 SCANNING REFERENCE ELECTRODE TECHNIQUE (SRET)</b>	<b>41</b>
<b>SCANNING VIBRATING ELECTRODE TECHNIQUE (SVET)</b>	

2.4.1 Introduction	45
<b>2.5 RAMAN SPECTROSCOPY</b>	<b>47</b>
<b>CHAPTER 3- MATERIAL SYNTHESIS AND CHARACTERISATION</b>	<b>49</b>
<b>3.1 INTRODUCTION</b>	<b>49</b>
<b>3.2 MATERIALS</b>	<b>50</b>
3.2.1 Monomer purification	50
3.2.2 Reagents	50
3.2.3 Solvents and aqueous acids	50
<b>3.3 PREPARATION OF POLYANILINE-HCSA/POLY(BUTYL ACRYLATE-VINYL ACETATE) COPOLYMER COMPOSITE</b>	<b>51</b>
<b>3.4 PREPARATION OF POLY(3-OCTYL PYRROLE)</b>	<b>53</b>
3.4.1 Electrochemical polymerisation	53
3.4.2 Chemical polymerisation	54
<b>3.5 MATERIAL CHARACTERISATION</b>	<b>55</b>
3.5.1 Solubility	55
3.5.2 Cyclic Voltammetry	55
3.5.3 Ultraviolet-visible spectroscopy	56
3.5.4 Raman Spectroscopy	56
3.5.5 Electrical conductivity measurement	56
<b>3.6 COATING PREPARATION</b>	<b>57</b>
3.6.1 Surface treatment	57
3.6.2 Coating of substrate	58
3.6.2.1 Air brushing	58

3.6.2.2 <i>Evaporative casting</i>	58
<b>3.7 COATING CHARACTERIZATION</b>	<b>58</b>
3.7.1 <i>Coating thickness</i>	58
3.7.2 <i>Coating adhesion</i>	59
<b>3.8 RESULTS AND DISCUSSION</b>	<b>60</b>
3.8.1 <i>Preparation and characterisation of Polyaniline/Poly(butyl acrylate- vinyl acetate) copolymer composite</i>	60
3.8.2 <i>Preparation and characterisation of Poly(3-octyl pyrrole)</i>	64
3.8.2.1 <i>Electrochemical synthesis of P3OP-pTS from 80/20 CCl<sub>4</sub>/DCM</i>	64
3.8.2.2 <i>Electrochemical synthesis of P3OP in AN</i>	66
3.8.2.3 <i>Electrochemical synthesis of poly(3-octyl pyrrole) in DCM</i>	68
3.8.2.4 <i>Chemical synthesis of P3OP-ClO<sub>4</sub> made in AN</i>	71
3.8.2.5 <i>Chemical synthesis of P3OP-pTs made in using Fe(pTS)<sub>3</sub> in MeOH</i>	75
3.8.3 <i>Coating characterisation</i>	76
3.8.3.1 <i>PAn/co-polymer coating</i>	76
3.8.3.2 <i>P3OP-pTS coating of electrochemical synthesis in 80/20 DCM/CCl<sub>4</sub></i>	77
3.8.3.3 <i>P3OP-TBAP coating of electrochemical synthesis in DCM</i>	77
3.8.3.4 <i>P3OP-pTS coating of electrochemical synthesis in DCM</i>	78
3.8.3.5 <i>P3OP-ClO<sub>4</sub> coating of chemical synthesis in AN</i>	78
3.8.3.6 <i>P3OP-pTS coating of chemical synthesis in MeOH</i>	79
<b>3.9 CONCLUSIONS</b>	<b>79</b>
<b>CHAPTER 4- ELECTROCHEMICAL CHARACTERISATION OF ICP COATED AA2024-T3</b>	<b>81</b>



<b>4.1 INTRODUCTION</b>	<b>81</b>
<i>4.1.1 EC of polyaniline coated steel</i>	<i>81</i>
<b>4.2 EXPERIMENTAL PROCEDURE</b>	<b>84</b>
<i>4.2.1 Sample preparations</i>	<i>84</i>
<i>4.2.2 Polarisation measurements</i>	<i>85</i>
<i>4.2.3 EIS and Open circuit potential (OCP) measurements</i>	<i>86</i>
<b>4.3 RESULTS AND DISCUSSION</b>	<b>88</b>
<i>4.3.1 Sample preparations</i>	<i>88</i>
<i>4.3.1.1 Open Circuit Potential (OCP)</i>	<i>88</i>
<i>4.3.1.2 Potentiodynamic polarisation</i>	<i>89</i>
<i>4.3.1.3 EIS of uncoated AA2024-T3</i>	<i>92</i>
<i>4.3.1.4 EIS of “Air dried” PAn/co-poly coated AA2024-T3</i>	<i>95</i>
<i>4.3.1.5 EIS of “Heat dried” PAn/co-poly coated AA2024-T3</i>	<i>99</i>
<i>4.3.2 Electrochemically synthesised Poly(3-octyl pyrrole) coated AA2024-T3</i>	<i>102</i>
<i>4.3.2.1 Open Circuit Potential (OCP)</i>	<i>103</i>
<i>4.3.2.2 EIS of “Ashraf” coated AA2024-T3</i>	<i>104</i>
<i>4.3.2.3 EIS of “P3OP-ClO4 deposit” coated AA2024-T3</i>	<i>107</i>
<i>4.3.2.4 EIS of “P3OP-ClO4 solution” coated AA2024-T3</i>	<i>111</i>
<i>4.3.2.5 EIS of “P3OP-pTS solution” coated AA2024-T3</i>	<i>114</i>
<i>4.3.3 Chemically synthesised Poly(3-octyl pyrrole) coated AA2024-T3</i>	<i>116</i>
<i>4.3.3.1 Open Circuit Potential (OCP)</i>	<i>117</i>
<i>4.3.3.2 Potentiodynamic polarisation</i>	<i>119</i>
<i>4.3.3.3 EIS of chemically synthesised P3OP-ClO4 coated on AA2024-T3</i>	<i>122</i>
<i>4.3.3.4 EIS of chemically synthesised P3OP-pTS coated AA2024-T3</i>	<i>125</i>
<b>4.4 CONCLUSIONS</b>	<b>127</b>

<b>CHAPTER 5- CHARACTERISATION OF LOCAL CORROSION</b>	<b>130</b>
<b>BEHAVIOUR FOR ICP COATINGS</b>	
<b>5.1 INTRODUCTION</b>	<b>130</b>
<b>5.2 EXPERIMENTAL PROCEDURES</b>	<b>133</b>
<b>5.3 RESULTS AND DISCUSSION</b>	<b>135</b>
<i>5.3.1 SVET of AA2024-T3</i>	<i>135</i>
<i>5.3.2 SVET of “air dried” Pan/co-polymer coated AA2024-T3 containing artificial defect</i>	<i>136</i>
<i>5.3.3 SVET of “heat dried” PAn/co-poly coated AA2024-T3 containing artificial defect</i>	<i>141</i>
<i>5.3.4 SVET of electrochemically synthesised POP-pTS coated AA2024-T3 containing artificial defect</i>	<i>143</i>
<i>5.3.5 SVET of chemically synthesised POP-ClO<sub>4</sub> coated AA2024-T3 containing artificial defect</i>	<i>146</i>
<i>5.3.6 SVET of chemically synthesised POP-pTs coated AA2024-T3 containing an artificial defect</i>	<i>151</i>
<i>5.3.7 SVET of Zinc-55% Aluminium hot dip coated steel</i>	<i>153</i>
<i>5.3.8 SVET of Zinc-55% Aluminium hot dip coated steel with “deep” artificial defect</i>	<i>156</i>
<i>5.3.9 SVET of electrochemically synthesised POP-pTS on Zinc-55% Aluminium hot dip coated steel with “shallow” artificial defect</i>	<i>158</i>
<i>5.3.10 SVET of electrochemically synthesised POP-pTS on Zinc-55% Aluminium hot dip coated steel without artificial defect</i>	<i>161</i>
<i>5.3.11 SVET of electrochemically synthesised POP-pTS on Zinc-55%</i>	<i>163</i>

<i>Aluminium hot dip coated steel with “deep” artificial defect</i>	
<b>5.4 CONCLUSIONS</b>	<b>166</b>
<b>CHAPTER 6- CHARACTERISATION OF PAN/CO-POLY COATING</b>	<b>169</b>
<b>DURING THE CORROSION PROCESS</b>	
<b>6.1 INTRODUCTION</b>	<b>169</b>
<b>6.2 EXPERIMENTAL</b>	<b>171</b>
<i>6.2.1 Raman spectroscopy</i>	<i>171</i>
<i>6.2.2 Sample preparation</i>	<i>172</i>
<b>6.3 RESULTS AND DISCUSSION</b>	<b>173</b>
<i>6.3.1 In-situ Raman spectroscopy of PAN/co-poly coated Pt</i>	<i>173</i>
<i>6.3.2 In-situ Raman spectroscopy of PAN/co-poly coated Pt containing defect</i>	<i>175</i>
<i>6.3.3 In-situ Raman spectroscopy of PAN/co-poly coated AA2024-T3</i>	<i>177</i>
<i>6.3.4 In-situ Raman spectroscopy of PAN/co-poly coated Al2024T3 containing defect</i>	<i>178</i>
<i>6.3.4.1 Ambient conditions</i>	<i>178</i>
<i>6.3.4.2 N<sub>2</sub> Atmosphere</i>	<i>181</i>
<b>6.4 CONCLUSIONS</b>	<b>187</b>
<b>CHAPTER 7- CONCLUSIONS</b>	<b>189</b>
<b>7.1 MATERIAL SYNTHESIS, POLYMER AND COATING CHARACTERISATION</b>	<b>189</b>
<b>7.2 ELECTROCHEMICAL CHARACTERISATION OF ICP COATED AA2024-T3</b>	<b>191</b>

<b>7.3 CHARACTERISATION OF LOCAL CORROSION BEHAVIOUR FOR ICP COATINGS</b>	<b>193</b>
<b>CHAPTER 8- REFERENCES</b>	<b>196</b>
<b>APPENDIX A</b>	<b>207</b>

## LIST OF FIGURES

Figure 1.1 Schematic of electrochemical corrosion cell where a potential difference between the two sites drives the current.

Figure 1.2 The interactions of chromate on an Al surface. [10]

Figure 1.3 Schematic representation of the polymerization of pyrrole to give polypyrrole with the incorporation of a dopant anion  $A^-$ .

Figure 1.4 Mechanism of polypyrrole polymerisation. [57]

Figure 1.5 Reaction steps in electrochemical polymerisation of aniline forming polyaniline. [14]

Figure 1.6 Reaction steps in chemical polymerisation of aniline forming polyaniline. [14]

Figure 1.7 Redox reaction of PPy with expulsion of dopant anion upon reduction.

Figure 1.8 Redox reaction of PPy with inclusion of cation upon reduction.

Figure 1.9 Protonation and redox reactions between various forms of PAn [14]

Figure 2.1 A schematic representation of Potentiodynamic scanning (PDS) (Black) with open circuit Potential (OCP), passivation potential ( $E_{pp}$ ), breakdown potential

(E<sub>b</sub>). cyclic polarisation (CP) with positive hysteresis (Black+red) and negative hysteresis (Black +blue) both with repassivation potential (E<sub>pp</sub>).

Figure 2.2 Sinusoidal current response to sinusoidal potential wave in a linear system.

Figure 2.3 Typical Nyquist plot for a corroding metal under charge transfer control. With impedance vector (arrow) of length  $|Z|$  and the angle between the vector and the x-axis is  $\phi$ . Frequency decreases from left to right.

Figure 2.4 Typical Bode plot for a corroding metal under charge transfer control.

Figure 2.5 Two different equivalent circuits with the same frequency response [85]

Figure 2.6 Schematic of the electric double layer of a corroding metal in electrolyte with corresponding EC.

Figure 2.7 Illustration a resistance model for a surface in an electrolyte and equipotential lines forming above a corroding metal with local anodic and cathodic sites.

Figure 2.8 Schematic energy diagram for Raman scattering

Figure 3.1 UV-vis spectra of PAn/co-polymer film after 20 min heat treatment. Films were formed by airbrushing polymer solution onto glass slide.

Figure 3.2 CV of PAn/co-polymer film after 20 min heat treatment Films were formed by airbrushing polymer solution onto a Pt electrode. CV was performed in 0.5 M HCl at 50 mV/s vs. Ag/AgCl.

Figure 3.3 Conductivity of PAn/co-polymer pellet after 20 min heat treatment.

Figure 3.4 Raman spectra of PAn/co-polymer film after 20 min heat treatment. Films were formed by airbrushing polymer solution onto glass slide.

Figure 3.5 UV-vis of P3OP-pTS solution fraction made by electrochemical polymerisation in DCM/CCl<sub>4</sub> (80/20 v/v) for different polymerisation times.

Figure 3.6 Chronopotentiogram of electrochemical polymerisation of P3OP-ClO<sub>4</sub> in AN using different current densities.

Figure 3.7 UV-vis of P3OP-ClO<sub>4</sub> in THF made by electrochemical polymerisation in AN using different current densities.

Figure 3.8 Chronopotentiogram of electrochemical polymerisation P3OP-ClO<sub>4</sub> in DCM using different current densities.

Figure 3.9 UV-vis of P3OP-ClO<sub>4</sub> in THF made by P3OP-ClO<sub>4</sub> made by electrochemical polymerisation in DCM using different current densities.

Figure 3.10 UV-vis of P3OP-ClO<sub>4</sub> made by addition of oxidant solution (Cu(ClO<sub>4</sub>)<sub>2</sub> in AN) to monomer solution (0.12 M OP in AN) using different oxidant/monomer ratio.

Figure 3.11 UV-vis of P3OP-ClO<sub>4</sub> made by addition of monomer solution (0.12 M OP in AN) to oxidant solution (Cu(ClO<sub>4</sub>)<sub>2</sub> in AN) solution using different oxidant/monomer ratio.

Figure 3.12 UV-vis of P3OP-pTS made by addition of monomer solution (0.12 M OP in MeOH) to oxidant solution ( $\text{Fe}(\text{pTS})_3$  in MeOH) solution using different oxidant/monomer ratio.

Figure 4.1 Equivalent circuit suggested by Schauer et al. for steel coated with a PAn blended primer covered by an epoxy topcoat tested in 0.5M NaCl. [96]

Figure 4.2 Equivalent circuit suggested by Li et al. for steel coated with a PAn blended primer without use of an insulating topcoat tested in 1 M HCl. [97]

Figure 4.3 Equivalent circuit suggested by Li et al. for steel coated with a PAn blended primer with use of an insulating topcoat tested in 1 M

Figure 4.4 Schematic of electrochemical cell used to perform polarisation, OCP and EIS experiments.

Figure 4.5 ECM commonly used for failed barrier coatings

Figure 4.6 OCP of AA2024-T3, AA2024-T3 coated with heat treated PAn/co-poly composite and 2024-T3 coated with air dried PAn/co-poly composite immersed in DHS vs. Ag/AgCl reference electrode

Figure 4.7 Cyclic polarisation curves for AA2024-T3 exposed to DHS with and without and heat treated PAn/co-poly composite coating. Scan initiated 30 min after immersion using a scan rate of 10 mV/min vs. Ag/AgCl reference electrode.



Figure 4.8 Cathodic polarisation curves for AA2024-T3 exposed to DHS with and without and heat treated PAn/co-poly composite coating. Scan initiated 30 min after immersion using a scan rate of 10 mV/min

Figure 4.9 Nyquist plot of uncoated AA2024-T3 immersed in DHS (exposed area: 2.5 cm<sup>2</sup>)

Figure 4.10 Bode plots of uncoated AA2024-T3 immersed in DHS (exposed area: 2.5 cm<sup>2</sup>)

Figure 4.11 ECM used model bare AA2024-T3 in DHS before 9 days immersion.

Figure 4.12 Nyquist plot of air dried PAn/co-poly coated AA2024-T3 immersed in DHS (exposed area: 2.5 cm<sup>2</sup>)

Figure 4.13 Nyquist plot of high frequency spectra of air dried PAn/co-poly AA2024-T3 immersed in DHS. The “developing” of the high frequency capacitive loop

Figure 4.14 Nyquist plot of air dried PAn/co-poly coated AA2024-T3 immersed in DHS (exposed area: 2.5 cm<sup>2</sup>)

Figure 4.15 ECM for “air dried” PAn/co-poly coated AA2024-T3 after 2 days exposure.

Figure 4.16 EC for “heat dried” PAn/co-poly coated AA2024-T3 after 2 days exposure.

Figure 4.17 Nyquist plot of heat exposed PAn/co-poly coated AA2024-T3 immersed in DHS (exposed area: 2.5 cm<sup>2</sup>)

Figure 4.18 Bode plots of heat exposed PAn/co-poly coated AA2024-T3 immersed in DHS (exposed area: 2.5 cm<sup>2</sup>)

Figure 4.19 Nyquist plot of high frequency spectra of heat exposed PAn/co-poly coated AA2024-T3 immersed in DHS (exposed area: 2.5 cm<sup>2</sup>)

Figure 4.20 OCP measurement of electrochemically synthesised P3OP coated AA2024-T3 immersed in DHS.

Figure 4.21 Nyquist plot of thin air brushed “Ashraf” coated AA2024-T3 immersed in DHS (exposed area: 2.5 cm<sup>2</sup>)

Figure 4.22 Bode plots of thin air brushed “Ashraf” coated AA2024-T3 immersed in DHS (exposed area: 2.5 cm<sup>2</sup>)

Figure 4.23 EC for thin air brushed “Ashraf” coated AA2024-T3 immersed in DHS

Figure 4.24 Nyquist plot 1 hour immersion of thin air brushed “P3OP-ClO<sub>4</sub> deposit” coated AA2024-T3 immersed in DHS (exposed area: 2.5 cm<sup>2</sup>)

Figure 4.25 EC for thin air brushed “P3OP-ClO<sub>4</sub> deposit” coated AA2024-T3 after 1 hour immersed in DHS.

Figure 4.26 Nyquist plot of thin air brushed “P3OP-ClO<sub>4</sub> deposit” coated AA2024-T3 immersed in DHS (exposed area: 2.5 cm<sup>2</sup>)

Figure 4.27 Bode plot of thin air brushed “P3OP-ClO<sub>4</sub> deposit” coated AA2024-T3 immersed in DHS (exposed area: 2.5 cm<sup>2</sup>)

Figure 4.28 Nyquist plot of high frequency end of thin air brushed “P3OP-ClO<sub>4</sub> deposit” coated AA2024-T3 immersed in DHS (exposed area: 2.5 cm<sup>2</sup>)

Figure 4.29 Nyquist plot 1 hour immersion of thin air brushed “P3OP-ClO<sub>4</sub> solution” coated AA2024-T3 immersed in DHS (exposed area: 2.5 cm<sup>2</sup>)

Figure 4.30 Nyquist plot of thin air brushed “P3OP-ClO<sub>4</sub> solution” coated AA2024-T3 immersed in DHS (exposed area: 2.5 cm<sup>2</sup>)

Figure 4.31 Bode plot of thin air brushed “P3OP-ClO<sub>4</sub> solution” coated AA2024-T3 immersed in DHS (exposed area: 2.5 cm<sup>2</sup>)

Figure 4.32 Nyquist plot of thin air brushed “P3OP-pTS solution” coated AA2024-T3 immersed in DHS (exposed area: 2.5 cm<sup>2</sup>)

Figure 4.33 Bode plot of thin air brushed “P3OP-pTS solution” coated AA2024-T3 immersed in DHS (exposed area: 2.5 cm<sup>2</sup>)

Figure 4.34 OCP for bare and P3OP coated AA2024-T3 exposed to DHS.

Figure 4.35 OCP for bare AA2024-T3 exposed to DHS with and without addition and 0.1 M NaClO<sub>4</sub> or 0.1 M NapTS.

Figure 4.36 Cyclic polarisation curves for bare and P3OP coated AA2024-T3 exposed to DHS. Scan initiated 30 min after immersion using a scan rate of 10 mV/min.

Figure 4.37 Cyclic polarisation curves for bare AA2024-T3 exposed to DHS. Scan initiated 30 min after immersion using a scan rate of 10 mV/min.

Figure 4.38 Cathodic polarisation curves for bare and P3OP coated AA2024-T3 exposed to DHS. Scan initiated 30 min after immersion using a scan rate of 10 mV/min.

Figure 4.39 Cathodic polarisation curves for bare AA2024-T3 exposed to DHS. Scan initiated 30 min after immersion using a scan rate of 10 mV/min.

Figure 4.40 Nyquist plot of cast “Chem. P3OP-ClO<sub>4</sub>” coated AA2024-T3 immersed in DHS (exposed area: 2.5cm<sup>2</sup>)

Figure 4.41 Bode plot of cast “Chem. P3OP-ClO<sub>4</sub>” coated AA2024-T3 immersed in DHS (exposed area: 2.5cm<sup>2</sup>)

Figure 4.42 Nyquist plot of cast “Chem. P3OP-pTS” coated AA2024-T3 immersed in DHS (exposed area: 2.5cm<sup>2</sup>)

Figure 4.43 Bode plot of cast “Chem. P3OP-pTS” coated AA2024-T3 immersed in DHS (exposed area: 2.5cm<sup>2</sup>)

Figure 5.1 Mechanistic view of pinhole passivation. PAn “anodises” exposed Fe surface. Dopant complexes with iron to form passive layer. ES= Emeraldine salt of PAn. LS= Leuco salt of PAn. DOP= Dopant anion. [105]

Figure 5.2 SVET current density distribution of AA2024-T3 in ambient DHS (data was collected by Dr. Jie He, NDSU, ND, USA.) Top left: 5 min immersion, Top right: 57 min immersion, Bottom left: 123 min immersion.

Figure 5.3 Mechanism of pitting corrosion of aluminium [107]

Figure 5.4 SVET of “air dried” PAn/co-poly coated AA2024-T3 containing artificial defect in ambient DHS. Left: Current density distribution Right: current vectors superimposed on optical image. Data collected after 10 minutes immersion.

Figure 5.5 SVET current density distribution and current vectors superimposed on optical image of “air dried” PAn/co-poly coated AA2024-T3 with artificial defect. Scan performed 40 minutes immersion in DHS.

Figure 5.6 SVET current density distribution and current vectors superimposed on optical image of “air dried” PAn/co-poly coated AA2024-T3 with artificial defect. Scan performed after 6 hours and 10 minutes immersion in DHS.

Figure 5.7 SVET current density distribution and current vectors superimposed on optical image of “air dried” PAn/co-poly AA2024-T3 with artificial defect. Scan performed after 9 hours and 10 minutes immersion in DHS.

Figure 5.8 SVET current density distribution and current vectors superimposed on optical image of “heat treated” PAn/co-poly coated AA2024-T3 with artificial defect. Scan performed after 3 minutes immersion in DHS.

Figure 5.9 SVET current density distribution and current vectors superimposed on optical image of “heat treated” PAn/co-poly coated AA2024-T3 with artificial defect. Scan performed after 2 hours and 33 minutes immersion in DHS.

Figure 5.10 Current density distribution and current vector superimposed on optical image of “heat treated” PAn/co-poly coated AA2024-T3 with artificial defect. Scan performed after 25 hours and 33 minutes immersion in DHS.

Figure 5.11 SVET current density distribution and current vectors superimposed on optical image of AA2024-T3 coated electrochemically synthesised P3OP-pTS containing an artificial defect. Scan performed in DHS after 1 hour 7 min.

Figure 5.12 SVET current density distribution and current vectors superimposed on optical image of AA2024-T3 coated electrochemically synthesised P3OP-pTS containing an artificial defect. Scan performed in DHS after 4 hours 37 min.

Figure 5.13 SVET current density distribution and current vectors superimposed on optical image of AA2024-T3 coated electrochemically synthesised P3OP-pTS containing an artificial defect. Scan performed in DHS after 20 hours 37 min.

Figure 5.14 AA2024-T3 coated chemically synthesised P3OP-ClO<sub>4</sub> containing an artificial defect. Scan performed in DHS. Upper left: 10 min. Upper right: current vector superimposed on optical image 10 min.

Figure 5.15 AA2024-T3 coated chemically synthesised P3OP-ClO<sub>4</sub> containing an artificial defect. Scan performed in DHS. Left: 5hours immersion. Right: 73hours immersion

Figure 5.16 Left: Current density distribution Right: optical image of AA2024-T3 coated with chemically synthesised P3OP-ClO<sub>4</sub> containing a wide artificial defect. Scan performed in DHS after 15 min

Figure 5.17 Left: Current density distribution Right: optical image of AA2024-T3 coated with chemically synthesised P3OP-ClO<sub>4</sub> containing a wide artificial defect. Scan performed in DHS after 3 hours 33 min. Bubble formation highlighted with drawn yellow ring in optical micrograph.

Figure 5.18 Left: Current density distribution Right: optical image of AA2024-T3 coated with chemically synthesised P3OP-ClO<sub>4</sub> containing a wide artificial defect. Scan performed in DHS after 44 hours 53 min

Figure 5.19 AA2024-T3 coated conducting, chemically synthesised P3OP-pTS containing an artificial defect after 3 min exposure in DHS

Figure 5.20 AA2024-T3 coated conducting, chemically synthesised P3OP-pTS containing an artificial defect after 1 hour 40 min exposure in DHS

Figure 5.21 AA2024-T3 coated conducting, chemically synthesised P3OP-pTS containing an artificial defect after 68 hours exposure in DHS.

Figure 5.22 SVET of bare Zinc-55 % Aluminium hot dip coated steel. Scan performed in DHS. Upper left: Current density map after 8 min exposure. Upper right: current vector superimposed on optical image after 8 min exposure. Lower left: Current density map after 4 hours 29 min exposure. Lower right: current vector superimposed on optical image after 4 hours 29 min exposure.

Figure 5.23 SVET of bare Zinc-55 % Aluminium hot dip coated steel. Scan performed in DHS. Left: Current density map after 20 hours 18 min exposure. Right: current vector superimposed on optical image after 20 hours 18 min exposure.

Figure 5.24 SVET of bare Zinc-55 % Aluminium hot dip coated steel with deep penetrating defect exposing underlying steel. Scan performed in DHS. Left: Current density map after 12 min exposure. Right: current vector superimposed on optical image after 12 min exposure.

Figure 5.25 SVET of bare Zinc-55 % Aluminium hot dip coated steel with deep penetrating defect exposing underlying steel. Scan performed in DHS. Left: Current density map after 19 hours 48 min exposure. Right: current vector superimposed on optical image after 19 hours 48 min exposure.

Figure 5.26 SVET current density distribution and current vectors superimposed on optical image of coated Zinc-55 % Aluminium hot dip coated steel electrochemically synthesised P3OP-pTS containing a “shallow” artificial defect. Scan performed in DHS after 2 min.

Figure 5.27 SVET current density distribution and current vectors superimposed on optical image of coated Zinc-55 % Aluminium hot dip coated steel electrochemically synthesised P3OP-pTs containing a “shallow” artificial defect. Scan performed in DHS after 11 min.

Figure 5.28 SVET current density distribution and current vectors superimposed on optical image of coated Zinc-55 % Aluminium hot dip coated steel electrochemically synthesised P3OP-pTs containing a “shallow” artificial defect. Scan performed in DHS after 20 hours 49 min.

Figure 5.29 SVET current density distribution and current vectors superimposed on optical image of coated Zinc-55 % Aluminium hot dip coated steel electrochemically synthesised P3OP-pTS. Scan performed in DHS after 3 min

Figure 5.30 Current density distribution of coated Zinc-55 % Aluminium hot dip coated steel electrochemically synthesised P3OP-pTS. Scan performed in DHS after Left: 47 hours 38 min, Right: 68 hours 35 min.



Figure 5.31 SVET current density distribution and current vectors superimposed on optical image of coated Zinc-55 % Aluminium hot dip coated steel electrochemically synthesised P3OP-pTS containing a “deep” artificial defect. Scan performed in DHS after 14 min.

Figure 5.32 SVET current density distribution and current vectors superimposed on optical image of coated Zinc-55 % Aluminium hot dip coated steel electrochemically synthesised P3OP-pTS containing a “deep” artificial defect. Scan performed in DHS after 2 hours 35 min.

Figure 5.33 SVET current density distribution and current vectors superimposed on optical image of coated Zinc-55 % Aluminium hot dip coated steel electrochemically synthesised P3OP-pTS containing a “deep” artificial defect. Scan performed in DHS after 19 hours 49 min.

Figure 6.1 Raman spectroscopy of PAn/co-poly coated Pt. Dry and in-situ after immersion in DHS with an OCP of 220 mV.

Figure 6.2 Raman spectroscopy of PAn/co-poly coated Pt immersed in DHS at OCP for 24 hours under N<sub>2</sub> and ambient conditions.

Figure 6.3 Relative intensity ratio of bands at 1610 cm<sup>-1</sup>/1590 cm<sup>-1</sup> as a function of distance to a coating defect.

Figure 6.4 Raman spectra of PAn/co-poly on AA2024-T3 as a function of immersion time in DHS performed under ambient conditions

Figure 6.5 Optical image of scribed PAn/co-polymer coating on AA2024-T3 in DHS after 15 min immersion using x10 magnification with area of Raman mapping are superimposed.

Figure 6.6 In-situ Raman spectroscopy of PAn/co-poly coated AA2024-T3 in DHS under ambient conditions with coating containing artificial defect. Spectra recorded after 10 min immersion. Black: 250  $\mu\text{m}$  distance from defect, Red: At the very edge of the coating, Blue: Point within the defect. Immersion time: 10 min.

Figure 6.7 In-situ Raman map of the peak area ratio of  $1610\text{ cm}^{-1}/1590\text{ cm}^{-1}$  of a scribed PAn/co-poly on AA2024-T3 immersed in DHS. Peak area was obtained with Gaussian peak fitting after intensity was normalised using the sum of the two peaks. TL: 15 min, TR: 1 hour, ML: 1 hour 40 min, MR: 5 hours 25 min, BL: 6 hours, BR: 7 hours 30 min

Figure 6.8 Optical image of scribed PAn/co-poly coating on AA2024-T3 in DHS after prior to immersion using x50 magnification with superimposed points where Raman spectra was recorded.

Figure 6.9 In-situ Raman spectroscopy of PAn/co-poly coated AA2024-T3 relative to an artificial defect recorded prior to immersion.

Figure 6.10 In-situ Raman spectroscopy of PAn/co-poly coated AA2024-T3 in DHS under  $\text{N}_2$  atmosphere with coating containing artificial defect. Spectra recorded after 15 min immersion.

Figure 6.11 In-situ Raman spectroscopy of PAn/co-poly coated AA2024-T3 in DHS under N<sub>2</sub> atmosphere with coating containing artificial defect. Spectra recorded after 60 min immersion.

Figure 6.12 In-situ Raman spectroscopy of PAn coated AA2024-T3 in DHS under N<sub>2</sub> atmosphere with coating containing artificial defect. Spectra recorded after 3 hours 30 min immersion.

Figure 6.13 In-situ Raman spectroscopy of PAn/co-poly coated AA2024-T3 in DHS under N<sub>2</sub> atmosphere with coating containing artificial defect. Spectra recorded after 7 hours immersion.

## LIST OF TABLES

Table 1.1 Composition in % of AA2024-T3 in addition to aluminium [1]

Table 1.2 Typical conducting polymer structures (in undoped form). [14]

Table 2.1 Impedance element and their expression

Table 3.1 Composition used for synthesis of poly(butyl acrylate-vinyl acetate) copolymer

Table 3.2 Solvents used to solute polymer material

Table 3.3 Solubility of PAn/co-polymer/co-poly in various solvents

Table 3.4 Effect of current density and charge passed on conductivity, yield and solubility of P3OP made by electrochemical polymerisation in AN.

Table 3.5 Effect of current density and charge passed on conductivity, yield and solubility of P3OP made by electrochemical polymerisation in DCM.

Table 3.6 Effect oxidant/monomer ratio on conductivity, yield and solubility of P3OP-ClO<sub>4</sub> made by addition of oxidant solution (Cu(ClO<sub>4</sub>)<sub>2</sub> in AN) to monomer solution (0.12 M OP in AN).

Table 3.7 Effect oxidant/monomer ratio on conductivity, yield and solubility of P3OP-ClO<sub>4</sub> made by addition of monomer solution (0.12 M OP in AN) to oxidant solution (Cu(ClO<sub>4</sub>)<sub>2</sub> in AN) solution.

Table 3.8 Effect oxidant/monomer ratio on conductivity and yield of P3OP-pTS made by addition of monomer solution (0.12 M OP in MeOH) to oxidant solution (Fe(pTS)<sub>3</sub> in MeOH) solution.

Table 4.1 Description and labelling of materials examined as corrosion inhibitors for AA2024-T3

Table 4.2 Description and labelling of materials examined as corrosion inhibitors for AA2024-T3

## ABSTRACT

Concern over the toxicity and environmental impact by use of chromate containing coating coatings has fuelled efforts to find suitable replacements. One class of materials considered as a potential replacement for chromate coatings are the intrinsically conducting polymers (ICP's). This thesis describes the synthesis and characterization of a range of ICP materials with emphasis on producing processable ICP and their use as corrosion protection coatings for aluminium alloy 2024-T3 and Zn-55%Al- hot dipped coated steel, two substrates that commonly employ chromate coatings for adequate protection. A general introduction to corrosion and ICP's are given in Chapter 1 with techniques employed to study corrosion inhibition detailed in Chapter 2.

Processability of Polyaniline was afforded by making of composite material to produce Polyaniline-HCSA/Poly(butyl acrylate-vinyl acetate) copolymer (PAn/co-poly) possessing moderate conductivity and electroactivity (Chapter 3). PAn/co-poly was highly soluble and could be applied as a coating to AA2024-T3 by airbrushing. Polypyrrole was afforded processability by monomer substitution to produce soluble Poly(3-octylpyrrole). Material synthesis was optimised to produce a maximum conductivity for the soluble ICP that could be applied to a metal surface by airbrushing or evaporative casting. Conductive, soluble P3OP was synthesised both through electrochemical and chemical synthesis P3OP route

Corrosion inhibition offered by ICP evaluated using Potentiodynamic polarisation and Electrochemical Impedance spectroscopy (EIS) (Chapter 4) suggests an interaction between the ICP coating and the underlying substrate. PAN/co-poly was observed to provide an anodic shift to the OCP of coated AA2024-T3. Increasing  $R_c$  and  $R_{ct}$  during exposure suggested that the coating converted towards a less conductive form. Exposure of conductive P3OP-ClO<sub>4</sub> coated AA2024-T3 also resulted in increasing  $R_{ct}$  overtime, ascribed to the formation of protective oxide.

Local corrosion behaviour within a coating defect was studied by SVET (Chapter 5). SVET demonstrated that PAN/co-poly accelerated corrosion within a defect without formation of protective oxide. Conductive fractions of P3OP exhibited decreasing oxidation within coating defect overtime suggesting the formation of an oxidation product that hinders further corrosion. Raman spectroscopy (Chapter 6) as well as visual observations (Chapter 4 and 5) suggest that oxidation of the substrate was promoted by the ICP that undergoes reduction. For P3OP this leads to lower corrosion current density within surface a defect suggesting that P3OP does protect against corrosion through anodic protection.

## ACKNOWLEDGMENTS

This thesis, the conclusion of several years work, is a result that I could not have achieved without the support of many people to whom I would like to express my gratitude.

Foremost I would like to express gratitude towards my supervisors; Professor Gordon Wallace and Doctor Peter Innis to whom I am deeply indebted. Only with their insight, encouragement and unwavering support far beyond the call of duty has this work been possible.

I would also like to extend my appreciation to Professor Dennis E. Tallman (North Dakota State University, USA) who has allowed me to visit and work with the NDSU corrosion group as well as being an exceptionally good host during my visits. I furthermore wish to extend my appreciation to staff and student of the corrosion group at North Dakota State University, USA. In particular Doctor Jie He for providing training and assistance in operation of the SVET instrument. I would also like to acknowledge Dr. Evan Evans from BlueScope Steel Limited for his support during this entire project. Also special thanks to all staff and students at IPRI for creating a friendly and positive work environment.

This work was produced with the financial assistance of the Australian Research Council and BlueScope Steel Limited.